Journal of Photochemistry and Photobiology A: Chemistry 201 (2009) 45–49

Contents lists available at ScienceDirect

Journal of Photochemistry and Photobiology A: Chemistry

journal homepage: www.elsevier.com/locate/jphotochem

TiO_2 nanotubes as recyclable catalyst for efficient photocatalytic degradation of indigo carmine dye

Leonardo L. Costa, Alexandre G.S. Prado*

Instituto de Química, Universidade de Brasília, Caixa Postal 4478, 70904-970 Brasília, Distrito Federal, Brazil

ARTICLE INFO

Article history:
Received 11 April 2008
Received in revised form
21 September 2008
Accepted 26 September 2008
Available online 15 October 2008

Keywords:
Nanotubes
TiO_2
Photodegradation
Indigo carmine

ABSTRACT

TiO_2 nanotubes have been synthesized in a hydrothermal system. The nanotubes were characterized by scanning electronic microscopy (SEM), FT-Raman spectroscopy and surface charge density by surface area analyzer. These nanocatalysts were applied to photocatalyse indigo carmine dye degradation. Photodegradation ability of TiO_2 nanotubes was compared to TiO_2 anatase photoactivity. Indigo carmine dye was completely degraded at 60 and 110 min of reaction catalysed by TiO_2 nanotubes and TiO_2 anatase, respectively. TiO_2 nanotubes presented high photodegradation activity at pH 2 and TiO_2 anatase at pH 4. TiO_2 nanotubes were easily recycled whereas the reuse of TiO_2 anatase was not effective. Nanotubes maintained 90% of activity after 10 catalytic cycles and TiO_2 anatase presented only 10% of its activity after 10 cycles.

1. Introduction

Many semiconductors have been used in heterogeneous photocatalysis. However, titanium(IV) oxide (titania) has been extensively applied as a photocatalyst due to its high stability and semiconductor abilities capable of generating charge carriers by absorbing energy [1–5].

The application of TiO_2 in photocatalysis and the mechanisms which involve these processes have also been discussed in several papers in the literature [6–8]. TiO_2 has three crystal phases: anatase, rutile, and brookite. However, only anatase phase shows good photocatalytic activity [9]. On the other hand, TiO_2 has two major disadvantages: (i) a relative large dosage of catalyst is needed and (ii) after photocatalysis processes it is difficult to recover the catalyst by filtration [10].

Separation of TiO_2 from effluents after dye degradation is very difficult due to its fine size and high stability of its hydrocolloid [11]. Hence, it needs a very costly filtration process before its disposal. Immobilization of TiO_2 on transparent supports and the modification of other metal ions have been developed in order to solve the problems with separation of TiO_2 from effluents [12,13].

Many researchers report several methods to develop nanosized TiO_2 in order to improve the photocatalytic abilities of this oxide [14,15]. Since the discovery of carbon nanotubes in the early 1990s, a new research area in material science was opened, and nanosized materials such as: nanoparticles, nanotubes, nanospheres and nanofibers, generally present new properties and behaviors, as well as better photocatalytic abilities than micro and macro materials [16].

Nanotubes obtained from TiO_2 have also been synthesized by many routes by using porous anodic alumina or organogel as templates via a sol–gel process. However, these nanotubes generally have large diameters, and their walls are composed of nanoparticles. High quality TiO_2 nanotubes have been obtained via simple hydrothermal treatment of crystalline TiO_2 particles with NaOH aqueous solutions [17,18].

In this direction, TiO_2 nanotubes were synthesized, characterized and applied to the photodegradation of indigo carmine dye. Recycling studies were followed and compared to traditional TiO_2 anatase photocatalyst in order to demonstrate the advantages of nanostructured TiO_2 in photocatalysis.

2. Experimental

2.1. Chemicals

TiO_2 (anatase) (Acros), indigo carmine dye (Vetec), NaOH (Vetec), NaCl (Vetec), and HNO_3 (Vetec) were used without further purification.

2.2. TiO_2 nanotubes synthesis

The titania nanotubes were synthesized by a hydrothermal reaction between NaOH solution and TiO_2 anatase. A total of 2 g of TiO_2

* Corresponding author. Fax: +55 61 32734149.
E-mail address: agspradus@gmail.com (A.G.S. Prado).

1010-6030/$ – see front matter © 2008 Elsevier B.V. All rights reserved.
doi:10.1016/j.jphotochem.2008.09.014

was suspended in 25 mL of 10 mol/L NaOH aqueous solution. This suspension was stirred for 15 min at room temperature and the mixture was reacted in an autoclave at 150 °C for 72 h. The obtained material was washed with H_2O and filtered off. This washed material was suspended in 500 mL of HCl aqueous solution at pH 2 and stirred for 24 h. HCl treatment was repeated 3 times in order to remove residual Na ions. After the HCl treatment, the suspension was centrifuged in order to separate the nanocatalyst from suspension.

2.3. Characterization

Scanning electron microscopy (SEM) was performed on a Zeiss EVO 50 microscope. Samples were coated with carbon using a metalliser Baltec SCD 50. Apparatus was operated at 20 keV.

Surface area was calculated by the Brunauer–Emmett–Teller (BET) method from Nitrogen adsorption–desorption data, which was measured on a Quantachrome Nova 2200 analyzer.

Infrared spectra of all samples were performed in KBr pellets in the 4000–400 cm^{-1} region with a resolution of 4 cm^{-1}, by accumulating 64 scans using a MB-100 Bomem FTIR spectrophotometer.

FT-Raman spectra of the solid samples were obtained on a Brucker Equinox 55 equipped with a Raman accessory. The resulting spectra were the sum of 128 scans and the laser power was set to 200 mW with spectral resolution of 4 cm^{-1}.

Powder X-ray diffraction patterns were measured on a Rigaku model D/Max-2A/C diffractometer using CuKα radiation. All the samples were scanned in the 2θ range of 2–50° at a scan rate of 2° min^{-1}.

Surface charge density of TiO_2 catalyst as a function of pH was calculated by applying Eq. (1) using K_1 and K_2 values obtained from simultaneous potentiometric and conductimetric titrations [19,20]. These titrations were carried out with a 50.0 mL aqueous suspension of TiO_2 nanotubes 40.0 g/L. Firstly, the TiO_2 nanotubes were fully deprotonated by addition of 0.4 mL of NaOH 1.0 mol/L. This sample was titrated with HNO_3 0.1 mol/L. The potentiometric readings were done with a pHmeter pHtek PHS-3B and the conductivity was measured by means of a Cole Parmer conductometer.

2.4. Indigo carmine photocatalytic degradation

The photolysis of indigo carmine dye was obtained in a homemade photoreactor [21] using 100.0 mL a 5×10^{-5} mol/L dye solution and 0.1 g/L of the photocatalysts TiO_2 nanotubes and TiO_2 anatase. These suspensions were illuminated by a mercury-vapour lamp "125 W" and the temperature was monitored during the reaction. The dye degradation was followed on a Beckman DU UV–vis spectrophotometer.

2.5. pH effect

100.0 mL of a 5×10^{-5} mol/L of dye solution and TiO_2 nanotubes 0.1 g/L were applied to degrade indigo carmine dye 1.0×10^{-5} mol/L at different pH values, which were adjusted by addition of HCl or NaOH. The irradiation in photoreactor was carried out during 60 min.

2.6. Recycling of TiO_2 nanotubes compared with TiO_2 anatase

After indigo carmine photodegradation, the photocatalysts were filtered by simple filtration using a filter paper Whatman Grade 42 with a pore size of 2.5 μm and washed with 300 mL of water. Then, they were added to a photoreactor to be reused in another indigo carmine dye solution, in order to perform the same photodegradation.

3. Results and discussion

3.1. Characterization

SEM images were carried out in order to understand the morphology of TiO_2 nanotubes. A representative scanning electron microscopic image of this photocatalyst obtained can be seen in Fig. 1, which shows that the TiO_2 nanotubes presented a diameter size of 20 nm.

Fig. 2 presents the N_2 isotherm of adsorption for TiO_2 anatase (Fig. 2B) and TiO_2 nanotubes (Fig. 2A). The isotherm of TiO_2 anatase shows that the adsorption–desorption processes are reversible, which is a typical characteristic of microporous material. On the other hand, this material presented a small hysteresis loop in the P/P_o range of 0.8–1.0, showing that the adsorption–desorption process is not reversible. This irreversibility is a consequence of capillary condensation in mesopores. Indeed, this isotherm shows that the TiO_2 nanotubes are predominantly formed by micropores with mesoporous sites forming an agglomerate structure [22–26].

The surface area values of catalysts were calculated by application of the BET equation in N_2 isotherms, which gave 8.0; and 76.0 $m^2\ g^{-1}$ for TiO_2 anatase and TiO_2 nanotubes, respectively. This fact evidences that the formation of nanotubes from TiO_2 anatase causes a significant increase on the surface area of the material, which is one of the new qualities of this nanocatalyst when compared with the start material.

Raman spectra of the precursor TiO_2 and titania nanotubes are presented in Fig. 3. The precursor TiO_2 spectrum presented only peaks related to the anatase phase at 141.7; 195.7; 396.2; 515.8; and 639.3 cm^{-1} [27,28]. Fig. 3b also shows peaks assigned to anatase phase of the nanotubes at 153.2; 191.8; 605.6 and 671.3 cm^{-1} [27,28]. However, this spectrum showed other characteristic peaks of nanotubular structure at 269.0; 446.4; and 671.3 cm^{-1} [29,30]. The bands at the 446.4 peak were assigned to a pure framework Ti–O–Ti vibration of rutile phase and the peaks at 269.0 and 671.3 cm^{-1} were assigned to the Ti–O–H bonds in interlayer regions of nanotube walls of rutile phase [29–33].

DRX patterns are presented in Fig. 4. Precursor TiO_2 presented a broad reflections at 2θ = 25, 37, 38, 39, 48, 54, 55, 63, 69, 70, and 75 related to anatase structure. On the other hand, TiO_2 nanotubes also showed reflections of anatase phase at 2θ = 25 and 49. Besides anatase peaks, one reflection at 2θ = 45 related to rutile phase was observed. Characteristic peaks of the nanotube formation at 2θ = 10, 31, and 61 related to $H_2Ti_3O_7$ were observed [30,32–34].

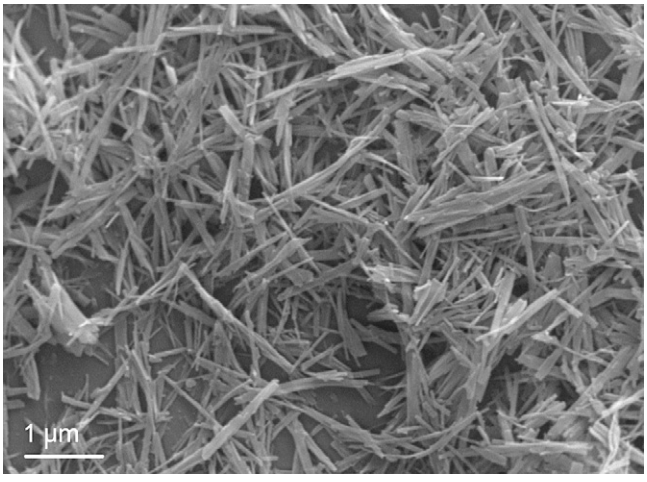

Fig. 1. SEM image of TiO_2 nanotubes.

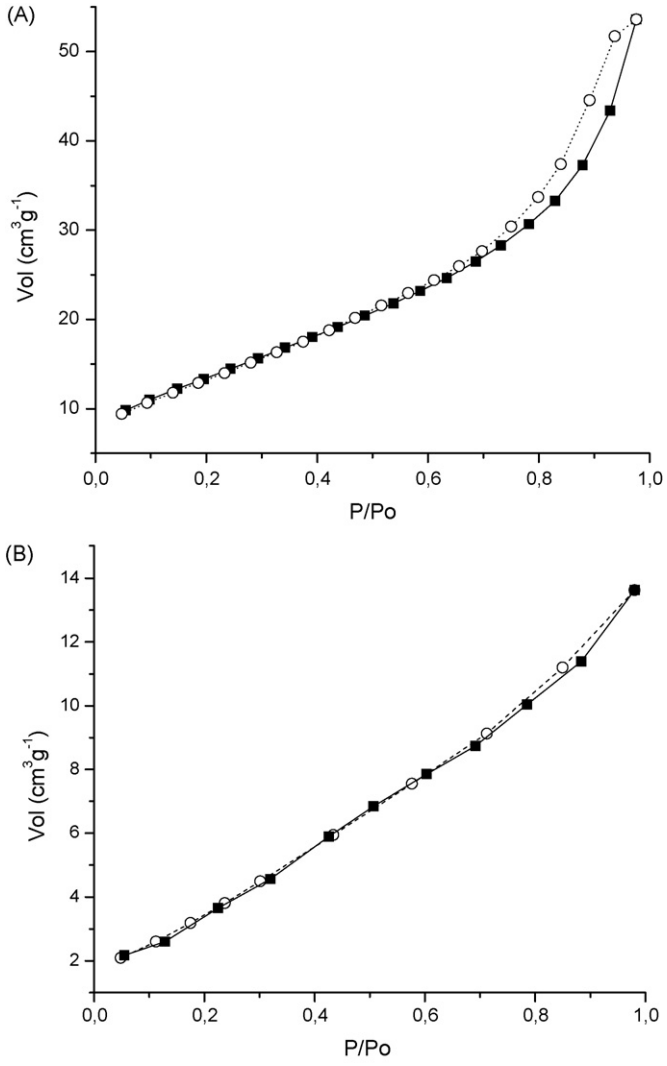

Fig. 2. Nitrogen adsorption–desorption isotherm for TiO_2 nanotubes (A) and TiO_2 anatase (B).

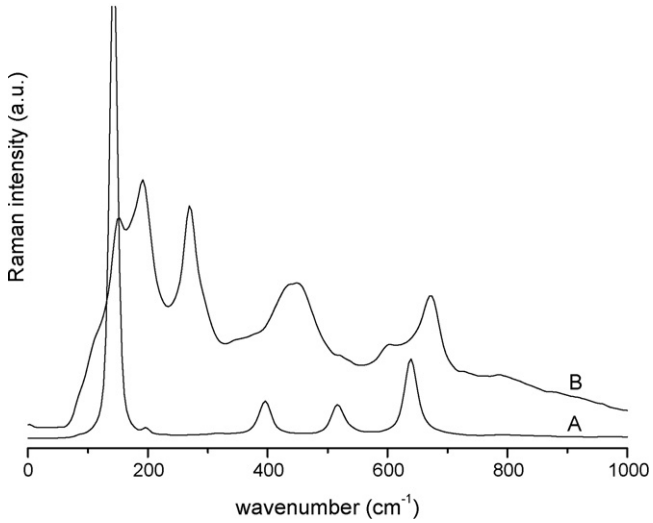

Fig. 3. FT-Raman spectra of the TiO_2 anatase (A) and titania nanotubes (B).

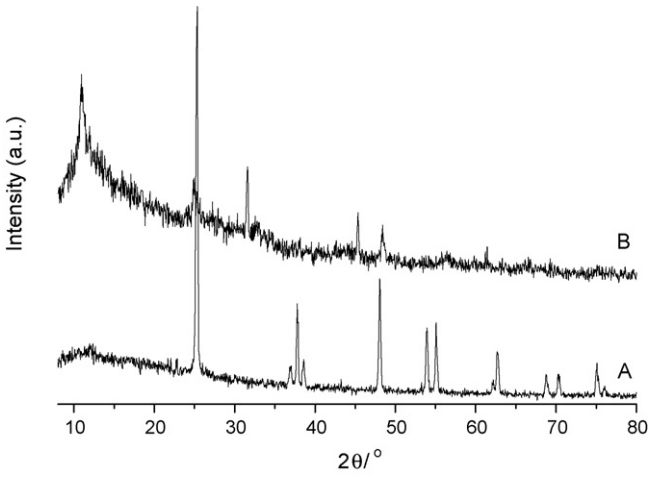

Fig. 4. DRX patterns for TiO_2 anatase (A) and TiO_2 nanotubes (B).

The suspension of oxides in aqueous solution must form distinct surface charge sites as a result of two steps of protonation of the surface groups by hydration of the oxide surface leading to three distinct surface sites as according to Eqs. (1) and (2) [19].

$$MOH_2^+ \rightarrow MOH + H^+; \quad K_1 \tag{1}$$

$$MOH \rightarrow MO^- + H^+; \quad K_2 \tag{2}$$

The surface of this material is dependent on pH values, which can present an acidified surface (MOH_2^+) in strong acidic medium, amphoteric surface sites (MOH) in intermediate media, and basic surface sites (MO^-) in strong basic medium. The equilibrium constants K_1 and K_2 can be experimentally determined by the application of the Henderson-Hasselbach equation in the simultaneous potentiometric and conductimetric titration data, as shown in Fig. 5. From equilibrium constants, the surface charge density of TiO_2 nanotubes as a function of pH values can be calculated by application of Eq. (3) [35,36].

$$\rho_0 = \left(\frac{F}{A}\right)\left[\frac{(10^{-2pH} - K_1K_2)}{(10^{-2pH} + 10^{-pH}K_1 + K_1K_2)}\right]N_T \tag{3}$$

where F is the Faraday constant, A is the total surface area, N_T is the total number of moles of surface sites, and K_1 and K_2 correspond to the acid equilibria constants.

Fig. 6 is plotted by applying Eq. (3). This figure shows three distinct regions. The first region is assigned to the protonated surface corresponding to the MOH_2^+ acid sites up to pH 5.9 and 4.0 for TiO_2 anatase and TiO_2 nanotubes, respectively. TiO_2 anatase presented a small region of amphoteric surface sites (MOH) between pH 5.9 and 6.4, whereas TiO nanotubes presented large amphoteric surface sites between pH 4.0 and 7.0. Above pH 6.4 and 7.0, it can be observed the deprotonated (MO^-) surface sites for TiO_2 anatase and TiO_2 nanotubes, respectively, can be observed. The point of zero charge (pzc) was observed at pH 6.2 and 5.6 for TiO_2 anatase and TiO_2 nanotubes, respectively.

3.2. Photocatalytic activity

The TiO_2 anatase is the main catalyst used in the contaminants photodegradation. However, the photocatalytic activity of TiO_2 nanotubes has been little explored in the literature [37,38]. Thus, a detailed study of the photocatalytic properties of TiO_2 nanotubes is necessary. In this direction, the degradation of indigo carmine dye was followed as a function of time in the presence of TiO_2 nanotubes and this dye degradation was also followed in the presence of TiO_2

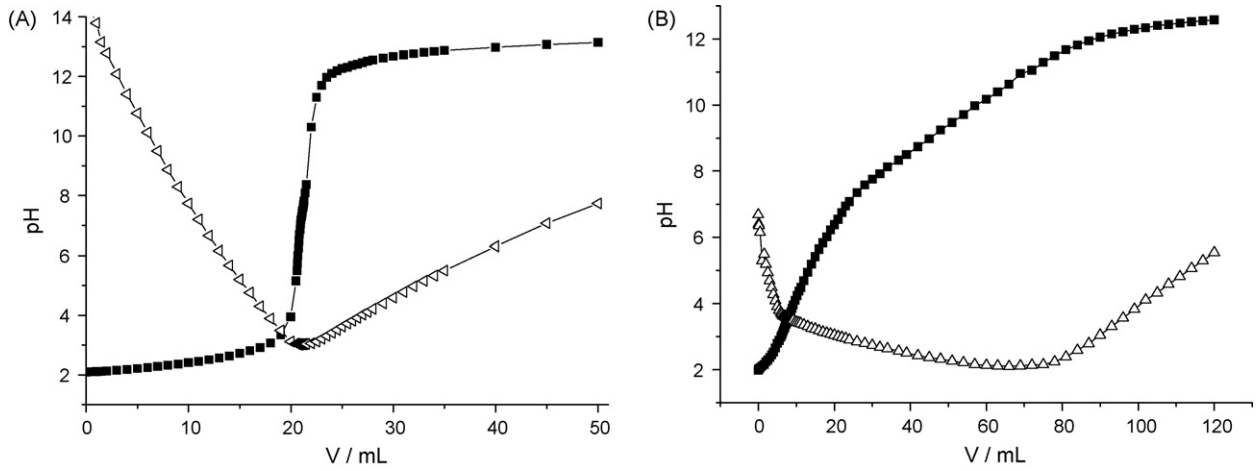

Fig. 5. Simultaneous conductimetric (■) potentiometric (Δ) titration curves of the suspensions of TiO_2 anatase (A) and titania nanotubes (B).

anatase in order to evaluate the photocatalytic ability of nanotubes in comparison with the key photocatalyst. Fig. 7 shows that TiO_2 presented high photocatalytic activity to degrade indigo carmine, degrading practically 100% of dye at 60 min of reaction, whereas the TiO_2 nanotubes degraded the dye only at 110 min. These results showed that TiO_2 acts faster than TiO_2 nanotubes even if taking into account that nanotubes present a surface area higher than TiO_2. This fact can be explained by the high stability of TiO_2 suspension in water, which increases the contact between contaminant and catalyst. Consequently, TiO_2 anatase presents photocatalytic activity higher than TiO_2 nanotubes, which was supported by the literature [39]. The effect of pH value in photocatalytic activity can be observed in Fig. 8.

The degradation was lower in basic medium for both catalysts. The degraded dye amount increases with the reduction of pH value. This behavior can be explained by the decrease of negative charge sites and by the increase of positive charge sites surfaces, which promotes a strong interaction with SO_3^- groups of the dye as according to studies of surface charge density as a function of pH values (Fig. 7). In the specific case of TiO_2 anatase, the highest activity was observed at pH 4 and below this value its activity decreased. Fig. 6 shows that below pH 4, the TiO_2 anatase surface is fully protonated. The addition of more acid in suspension at this pH must cause the increase of proton and chloride concentration, which can collapse the double layer to an extent that the ever-present attractive van der Waals forces overcome the charge repulsion [40]. As a consequence, the decrease of photocatalytic activity was observed in pH below 4.

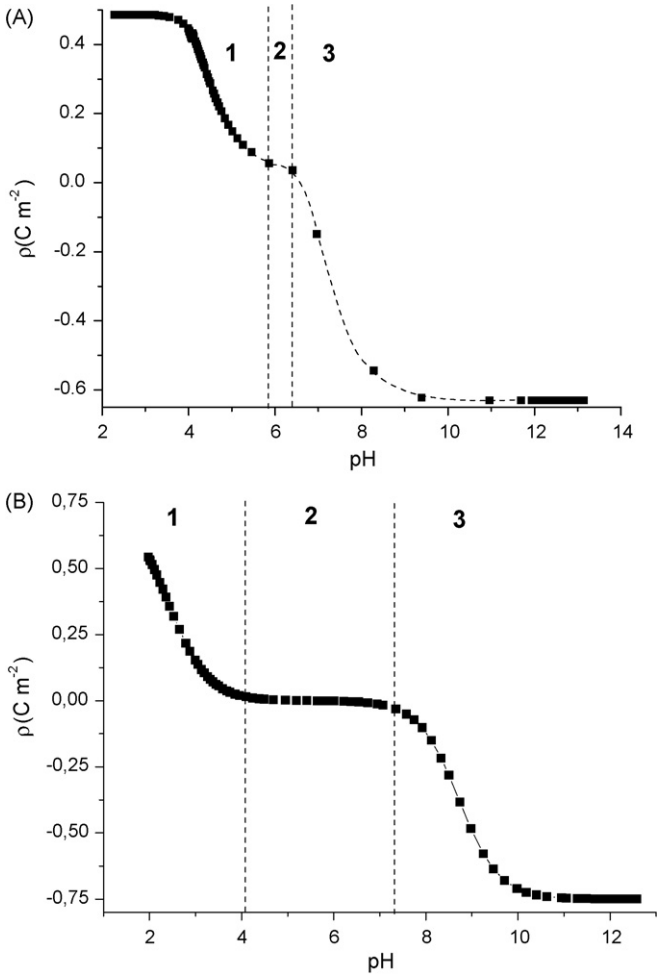

Fig. 6. Density surface charge as a function of pH for TiO_2 anatase and TiO_2 nanotubes. The region indexed 1, 2, and 3 correspond to the acidified surface (MOH_2^+), amphoteric surface sites (MOH), and basic surface sites (MO^-), respectively.

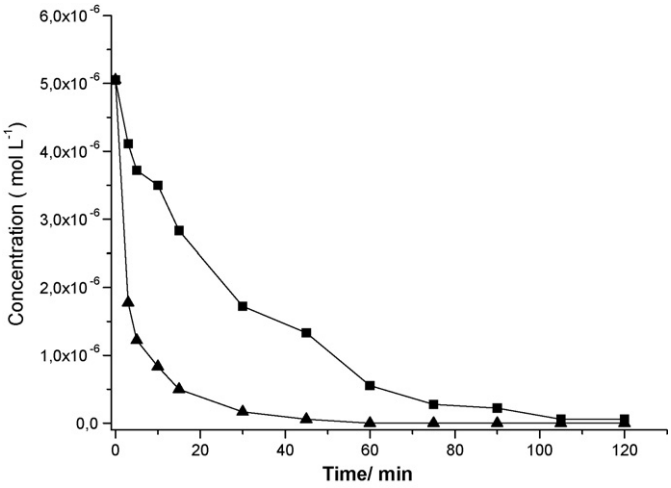

Fig. 7. Rates of photocatalysed degradation of the indigo carmine dye in the presence of TiO_2 anatase (▲) and TiO_2 nanotubes (■).

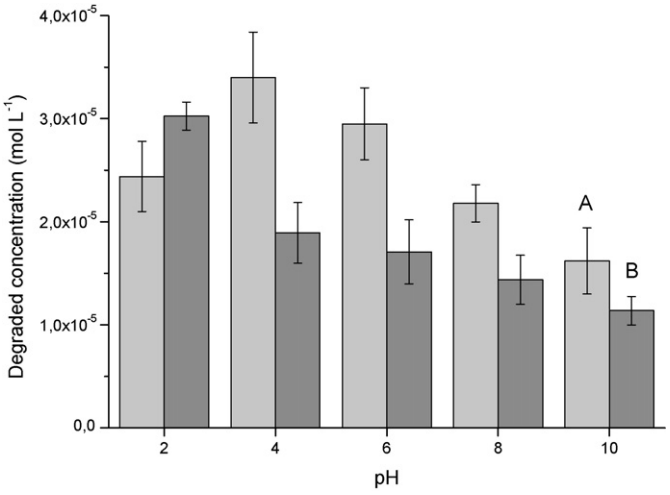

Fig. 8. The effect of pH value in photocatalytic activity of TiO_2 anatase (A) and TiO_2 nanotubes (B).

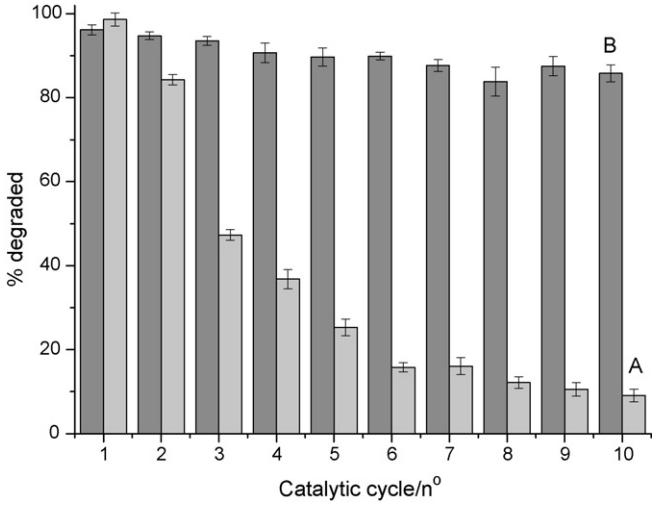

Fig. 9. Indigo carmine dye degradation for the recycling experiments of the TiO_2 anatase (A) and TiO_2 nanotubes photocatalysts (B).

The recycling studies were followed with TiO_2 anatase and TiO_2 nanotubes in order to compare the catalytic activity, as shown in Fig. 9. The filtration of TiO_2 nanotubes was very quick and easy, whereas the filtration of TiO_2 anatase was very slow and not efficient, due to a loss of approximately 15% of this catalyst during this procedure. These studies revealed that TiO_2 recovery is difficult and the re-application of these catalysts is not effective. The high stability of TiO_2 anatase in aqueous medium, which generates a high photocatalytic activity, makes its separation from reaction solution difficult. The activity of TiO_2 anatase decreased dramatically to 10% of dye degradation after 10 catalytic cycles, caused by the material loss during the recovering procedure. On the other hand, TiO_2 nanotubes were easily recycled and maintained 90% of dye degradation after 10 catalytic cycles, showing the TiO_2 nanotubes' ability to be reused in photodegradation reactions.

4. Conclusion

The synthesis of TiO_2 nanotubes is simple and occurred with success. TiO_2 nanotubes presented a photocatalytic activity lower than TiO_2 anatase to degrade indigo carmine dye. The nanotubes presented the best activity at pH 2 whereas TiO_2 anatase showed its highest activity at pH 4. The great advantage of TiO_2 nanotubes in comparison with traditional TiO_2 catalyst is its easy recovery. Consequently, the nanotubes can be recycled and re-applied in many photodegradation cycles, maintaining 90% of their activity after 10 cycles of reaction. The precursor TiO_2 catalyst lost its activity on the second catalytic cycle. Thus, the procedure presented here is according to the key principles of green chemistry.

Acknowledgments

The authors wish to thank CNPq and CAPES for financial support and for fellowships to AGSP and LLC.

References

[1] M.R. Hoffmann, S.T. Martin, W. Choi, D.W. Bahnemann, Chem. Rev. 95 (1995) 69–96.
[2] V.F. Stone, R.J. Davis, Chem. Mater. 10 (1998) 1468–1474.
[3] M. Adachi, Y. Murata, M. Harada, S. Yoshikawa, Chem. Lett. 8 (2000) 942–943.
[4] T. Sreethawong, Y. Suzuki, S. Yoshikawa, Catal. Commun. 6 (2005) 119–124.
[5] C.C. Tsai, J.N. Nian, H. Teng, Appl. Surf. Sci. 253 (2006) 1898–1902.
[6] I.K. Konstantinou, T.A. Albanis, Appl. Catal. B 49 (2004) 1–14.
[7] J.K. Zhou, Y.X. Zhang, X.S. Zhao, A.K. Ray, Ind. Eng. Chem. Res. 45 (2006) 3503–3511.
[8] A. Mills, R.H. Davies, D. Worsley, Chem. Soc. Rev. 22 (1993) 417–425.
[9] M.A. Fox, M.T. Dulay, Chem. Rev. 93 (1993) 341–357.
[10] S. Zhang, Z. Zheng, J. Wang, J. Chen, Chemosphere 65 (2006) 2282–2288.
[11] J.D. Torres, E.A. Faria, J.R. SouzaDe, A.G.S. Prado, J. Photochem. Photobiol. A 182 (2006) 202–206.
[12] C. Sahoo, A.K. Gupta, A. Pal, Dyes Pigm. 66 (2005) 189–196.
[13] V.M. Cristante, A.G.S. Prado, S.M.A. Jorge, J.P.S. Valente, A.O. Florentino, P.M. Padilha, J. Photochem. Photobiol. A 195 (2008) 23–26.
[14] B. Mahltig, E. Gutmann, E.C. Meyer, M. Reibold, B. Dresler, K. Gunther, D. Fassler, H. Bottcher, J. Mater. Chem. 17 (2007) 2367–2374.
[15] Y. Sakatani, D. Grosso, L. Nicole, C. Boissiere, G.J.D.A. Soler-Illia, C. Sanchez, J. Mater. Chem. 16 (2006) 77–82.
[16] L.M. Huang, Z. Jia, S. OïBrian, J. Mater. Chem. 17 (2007) 3863–3874.
[17] B.D. Yao, Y.F. Chan, X.Y. Zhang, W.F. Zhang, Z.Y. Yang, N. Wang, Appl. Phys. Lett. 82 (2003) 281–283.
[18] T. Kasuga, M. Hiramatsu, A. Hoson, T. Sekino, K. Niihara, Langmuir 14 (1998) 3160–3163.
[19] N. Kallay, T. Madic, K. Kucej, T. Preocanin, Colloid. Surf. A 250 (2004) 289–292.
[20] G.A. Parks, P.L.D Bruyn, J. Phys. Chem. 66 (1962) 967.
[21] L.B. Bolzon, J.R. SouzaDe, A.G.S. Prado, Rev. Bras. Ens. Quím 1 (2006) 25–32.
[22] E. DeOliveira, A.G.S. Prado, J. Mol. Catal. A 271 (2007) 63–69.
[23] P. Klobes, H. Preiss, K. Meyer, D. Shultze, Mikrochim. Acta 125 (1997) 343–347.
[24] E. DeOliveira, C.R. Neri, O.A. Serra, A.G.S. Prado, Chem. Mater. 19 (2007) 5437–5442.
[25] A.K.H. Nohman, H.M. Ismail, Colloid. Surf. A 136 (1998) 237–243.
[26] A.G.S. Prado, C. Airoldi, J. Mater. Chem. 12 (2002) 3823–3826.
[27] P.T. Hsiao, K.P. Wang, C.W. Cheng, H.S. Teng, J. Photochem. Photobiol. A 188 (2007) 19–24.
[28] L. Qian, Z.L. Du, S.Y. Yang, Z.S. Jin, J. Mol. Struct. 749 (2005) 103–107.
[29] J.A. Toledo-Antonio, S. Capula, M.A. Cortes-Jacome, C. Angeles-Chavez, E. Lopez-Salinas, G. Ferrat, J. Navarrete, J. Escobar, J. Phys. Chem. C 111 (2007) 10799–10805.
[30] M.A. Cortes-Jacome, G. Ferrat-Torres, L.F.F. Ortiz, C. Angeles-Chavez, E. Lopez-Salinas, J. Escobar, M.L. Mosqueira, J.A. Toledo-Antonio, Catal. Today 126 (2007) 248–255.
[31] M. Hodos, E. Horvath, H. Haspel, A. Kukovecz, Z. Konya, I. Kiricsi, Chem. Phys. Lett. 399 (2004) 512–515.
[32] A. Kukovecz, M. Hodos, Z. Konya, I. Kiricsi, Chem. Phys. Lett. 411 (2005) 445–449.
[33] D.V. Bavykin, J.M. Friedrich, A.A. Lapkin, F.C. Walsh, Chem. Mater. 18 (2006) 1124–1129.
[34] E. Horvath, A. Kukovecz, Z. Konya, I. Kiricsi, Chem. Mater. 19 (2007) 927–931.
[35] A.F.C. Campos, F.A. Tourinho, G.J. da Silva, M.C.F.L. Lara, J. Depeyrot, Eur. Phys. J. E 6 (2001) 29–35.
[36] A.G.S. Prado, L.B. Bolzon, C.P. Pedroso, L.L. DaCosta, Appl. Catal. B 82 (2008) 219–224.
[37] C.A. Grimes, J. Mater. Chem. 17 (2007) 1451–1457.
[38] D.V. Bavykin, V.N. Parmon, A.A. Lapkin, F.C. Walsh, J. Mater. Chem. 14 (2004) 3370–3377.
[39] Y.X. Yu, D.S. Xu, Appl. Catal. B 73 (2007) 166–171.
[40] W. Stumm, J.J. Morgan, Aquatic Chemistry: An Introduction Emphasizing Chemical Equilibria in Natural Waters, John Wiley & Sons, New York, 1981.